# Supplementary Information

## Selection of Phenyl hydrazine derivative as $Sn^{4+}$ reductant in Tin-Lead Perovskite Solar Cells

Yanjun Xing[a], Jiaxing Xiong[a], Qiuxiang Wang[a], Changlei Wang[b,*], Like Huang[a], Xiaohui Liu[a], Qidong Tai[c], Yuejin Zhu[a], Jing Zhang[a,*]

[a]Department of Microelectronic Science and Engineering, Ningbo University, Zhejiang, 315211, China.

[b]Department of Microelectronic Science and Engineering, Suzhou University, Suzhou, 215008, China.

[c]The Institute of Technological Sciences, Wuhan University, Wuhan 430072, PR China

**Experiment section**

Materials: Unless otherwise stated, all chemicals and materials are purchased and used on receipt. Lead iodide ($PbI_2$), PEDOT:PSS (Al 4083), methylammonium iodide (MAI), Formamidinium iodide (FAI), [6,6]-phenyl-C61-butyric acid methyl ester ($PC_{61}BM$) and 2,9- dimethyl-4,7-diphenyl-1,10-phenanthroline (BCP) from Xi'an Polymer Light Technology Corp. The tin iodide ($SnI_2$), tin fluoride ($SnF_2$), and guanidine thiocyanate (PbSCN), 3-(3,4Dihydroxyphenyl)-DL-alanine (DOPA), Sn powder are purchased from Aladdin.

$(FASnI_3)_{0.5}(MAPbI_3)_{0.5}$ Film preparation: The $FASnI_3$ solution is prepared by dissolving 0.3725 g of $SnI_2$, 0.172 g of FAI, and 0.0019 g of DOPA with 10 mol% of $SnF_2$ in DMF/DMSO (8:2). The $MAPbI_3$ precursor solution is prepared by dissolving 0.461 g $PbI_2$ and 0.159 g MAI with 5 mol% of PbSCN in DMF/DMSO (8:2). Excess Sn powder is added into the $FASnI_3$ solution precursor during the dissolution process, and then filter the solution by a 0.22 μm PVDF-filter. The $(FASnI_3)_{0.5}(MAPbI_3)_{0.5}$ precursor solution is then formed by mixing stoichiometric amounts of $FASnI_3$ and $MAPbI_3$ perovskite precursor. Adding a solvent with additives to the above-mentioned $FASnI_3$ solution, with a molar concentration of 4% additive (BH, HA and BHACl), can prepare a precursor solution of tin-lead mixed perovskite with a concentration of 2%.

**Device fabrication：**

The fluorine-doped tin oxide (FTO) glass substrate is ultrasonically cleaned with deionized water and alcohol, respectively, for 15 minutes at a time. PEDOT: PSS aqueous solution films are coated on the cleaned FTO substrate at 4000 rpm for the 30s

and then dried at 150 °C for 15 min. The $(FASnI_3)_{0.5}(MAPbI_3)_{0.5}$ solution is spin-coated onto the PEDOT: PSS substrate at 4000 rpm for 30 s, and CB is dropped onto the substrate at 20 s and then dried at 60 °C for 1 min and 100°C for 5 min. The PCBM solution of 20 mg $mL^{-1}$ in chlorobenzene is deposited on perovskite film at 3000 rpm for 30 s and then dried at 60 °C for 10 min. Finally, the 120 μL of BCP saturated solution is coated on the PCBM film at 5000 rpm and the Ag with a thickness of 80 nm to form an electrode through evaporation.

**Characterizations:**

Atomic force microscopy (AFM) is conducted on Veeco (America) and Kelvin probe force microscopy (KPFM) is used to detect the contact potential to reveal the fermi level and ion migration properties of the film under the bias applied normally to the film.

The surface morphology of the films and the cross-section morphology of the devices are tested by a Hitachi SU-70 scanning electron microscope (SEM). X-ray diffraction (XRD) patterns of films are tested by a Bruker D8 advanced instrument and using Cu Kα as radiation (λ=6.162Å) at a scan rate of $4°min^{-1}$ and diffraction angle range from 10° to 40°. The absorption spectra of the film on the glass substrate are measured by UV-visible spectrophotometer (Agilent, USA).

Proton nuclear magnetic resonance (1H NMR) is tested with Bruker AVANCE 600 MHz, and the lock solvent is deuterated dimethyl sulfoxide (DMSO-d6). FTIR spectroscopy are taken with FTIR spectrometer instrument (Thermo, Nicolet 6700). The binding energies of the elements in PVK are tested by X-ray photoelectron

spectroscopy (XPS, Shimadzu, Japan) using Al Kα radiation. Au is used to calibrating the energy state of the spectroscopy before measurement. The ultraviolet photoelectron spectroscopy (UPS) pattern is detected by the Axis Ultra DLD, and using the He I (21.22 eV) emission line. The steady-state fluorescence (PL) spectra of the films are measured based on the glass by a fluorescence spectrophotometer (Agilent, USA), with an excitation wavelength of 532 nm. The SCLC measurements and dark *J-V* curves are measured by the Keithley 4200 under condition.

The J-V characteristic curves are tested by the Keithley 4200 meter and the sunlight simulator (Newport, 91192A, AM 1.5, 1 sun) whose light intensity is calibrated by a standard silicon solar cell. The solar cells are masked with a black aperture to define the active area of 0.095 $cm^2$. The EQE is tested by Newport EQE system and wavelength range from 300 to 1100 nm. The transient photo-current (TPC) decay and transient photo-voltage (TPV) decay are recorded by an electrochemical workstation (Zahner, Germany) with a white light LED supplied 80 $mWcm^{-2}$ light intensity to excite the perovskite solar cells. EIS is also tested by an electrochemical workstation at a bias voltage of 0.6V.

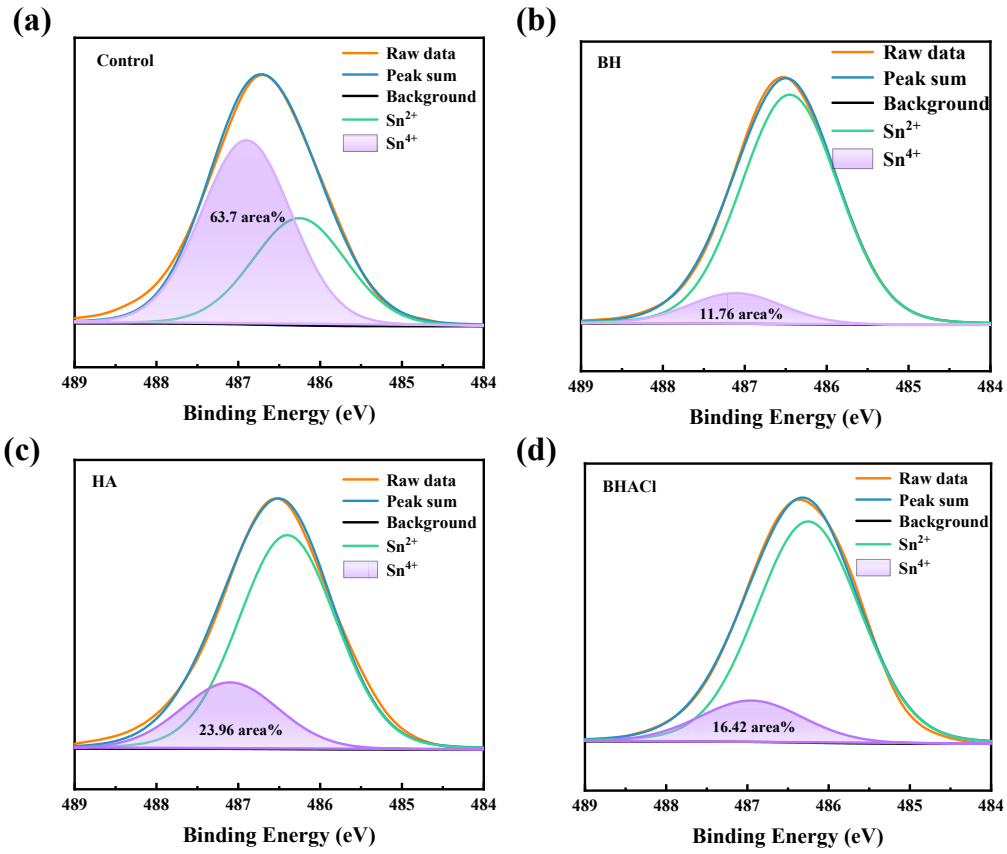


**Figure S1.** The XPS of (a) Control, (b) BH, (c) HA and (d) BHACl.

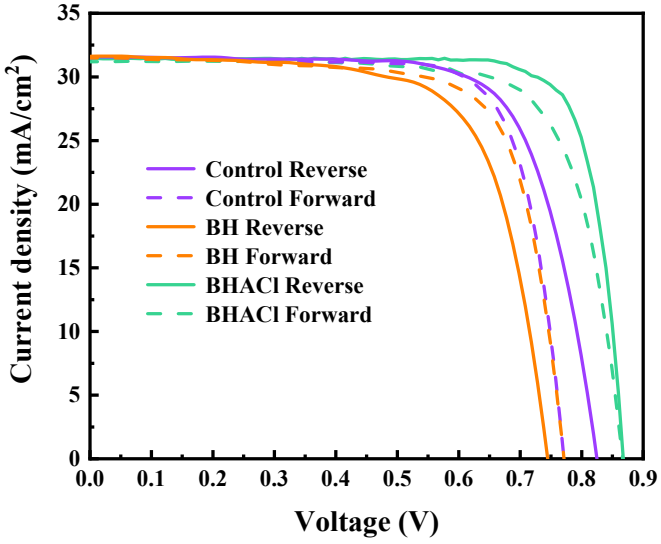


**Figure S2.** The hysteresis curve of Control, BH and BHACl.

**Table S1.** The photovoltaic parameters of Control, BH and BHACl devices.

| | | $V_{OC}$ (V) | $J_{SC}$ (mA/cm²) | FF (%) | PCE (%) |
|---|---|---|---|---|---|
| **Control** | **Forward** | 0.775 | 31.44 | 76.7 | 18.68 |
| | **Reverse** | 0.828 | 31.70 | 72.1 | 19.14 |
| **BH** | **Forward** | 0.776 | 31.29 | 74.6 | 18.11 |
| | **Reverse** | 0.748 | 31.47 | 69.4 | 16.33 |
| **BHACl** | **Forward** | 0.864 | 31.29 | 79.1 | 21.39 |
| | **Reverse** | 0.868 | 31.42 | 80.7 | 22.01 |

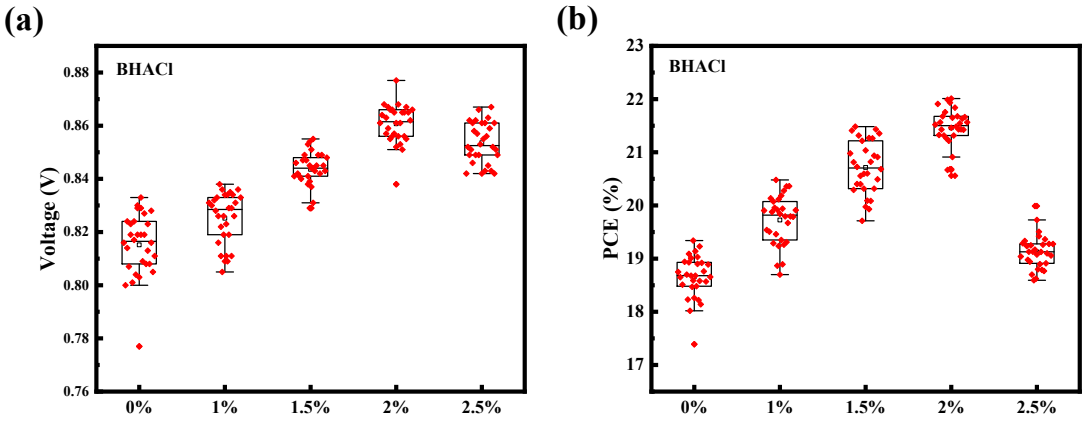


**Figure S3.** (a) Voltage and (b) PCE statistics of devices with different BHACl concentrations.

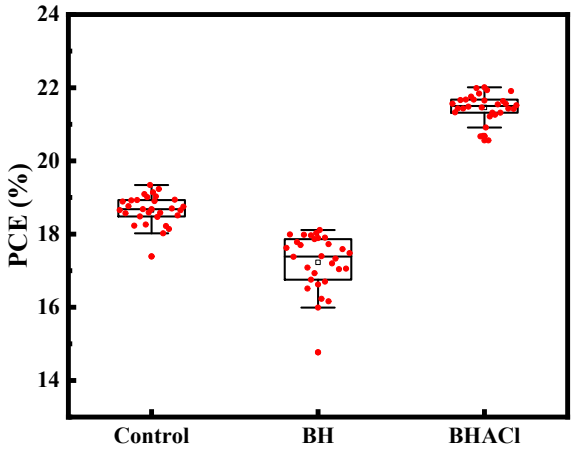


**Figure S4.** The PCE statistics of control, BH and BHACl devices.

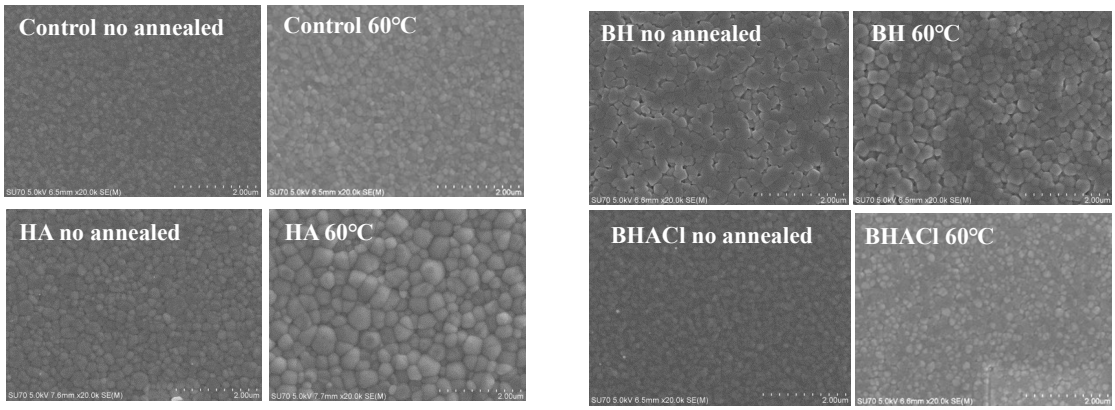


**Figure S5.** The SEM of Control, BH, HA and BHACl film during different annealing processes.

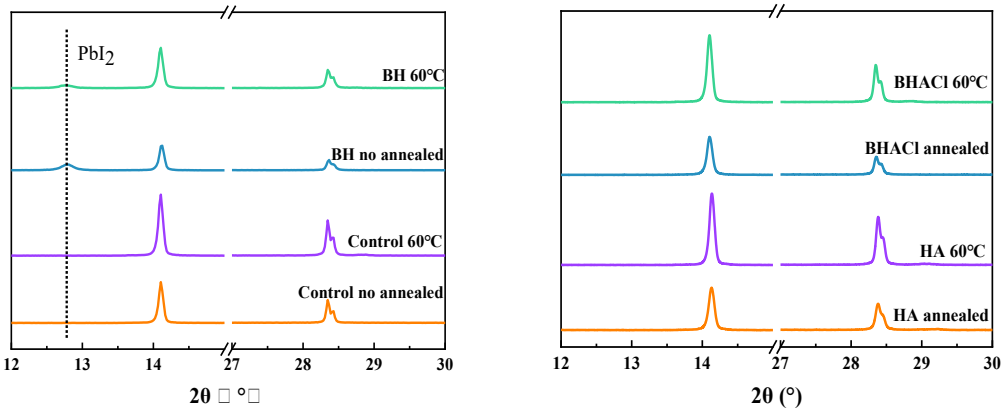


**Figure S6.** The XRD of Control, BH, HA and BHACl film during different annealing processes.

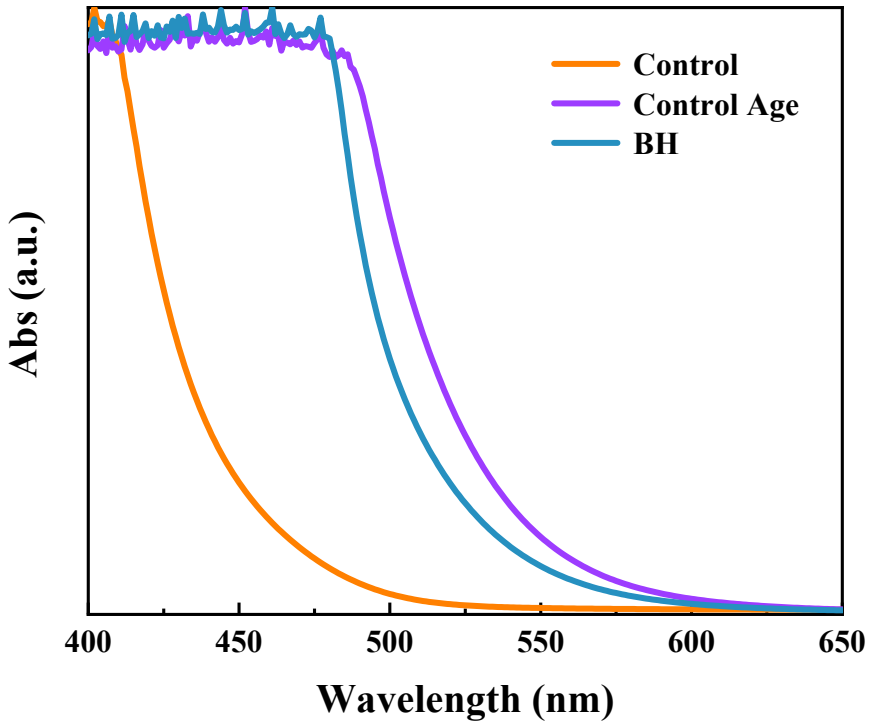


**Figure S7.** The UV-vis absorption of Control, Control age and BH solution.

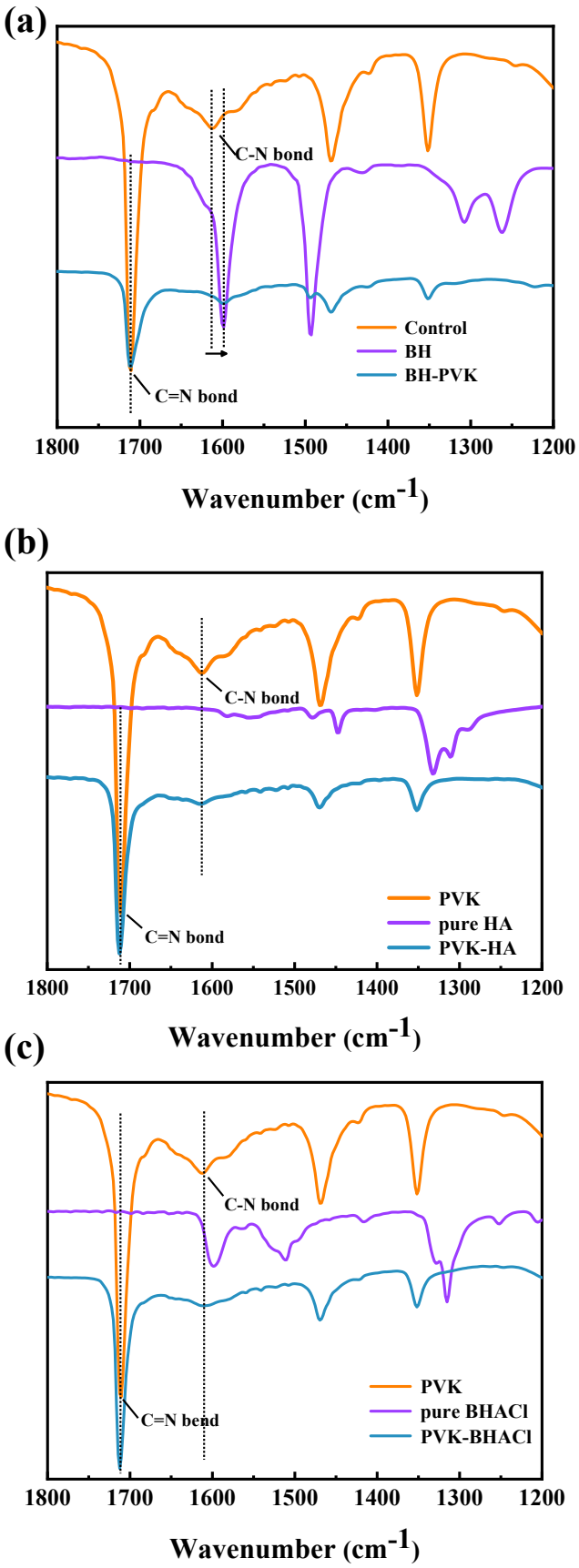


**Figure S8.** The FTIR of (a) BH, (b) BHACl and (c) HA film.

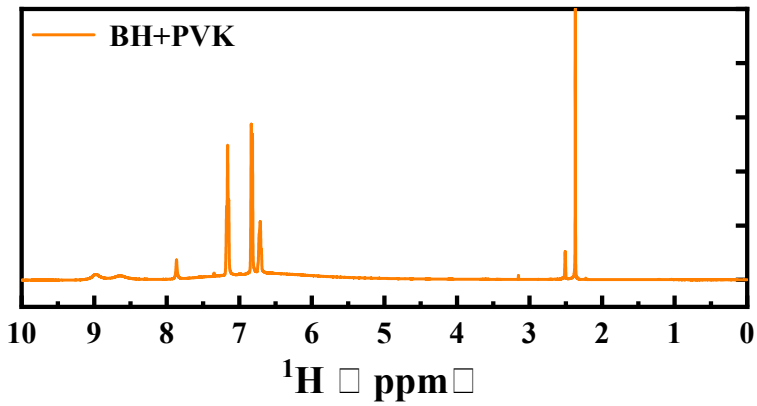


**Figure S9.** The $^{1}$H NMR of double the amount of perovskite solution in BH.

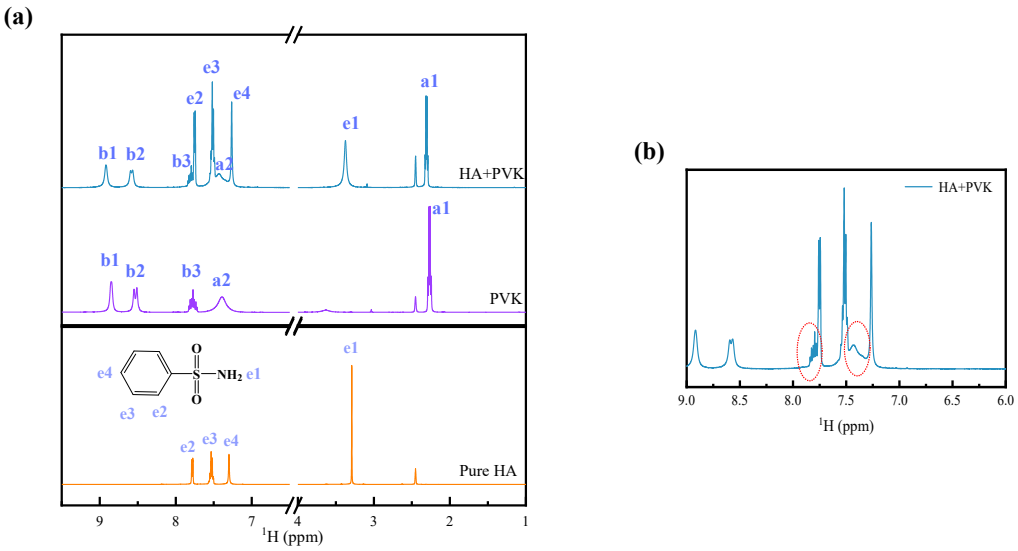


**Figure S10.** The $^{1}$H NMR of (a) HA and (b) HA+PVK.

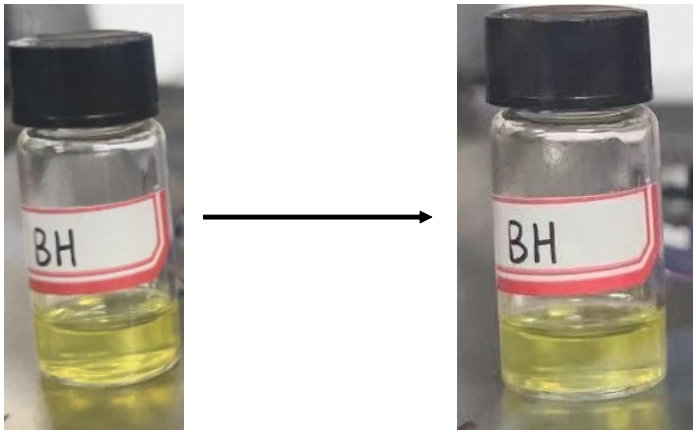


**Figure S11.** The $^{1}H$ NMR of (a) HA and (b) HA+PVK.+

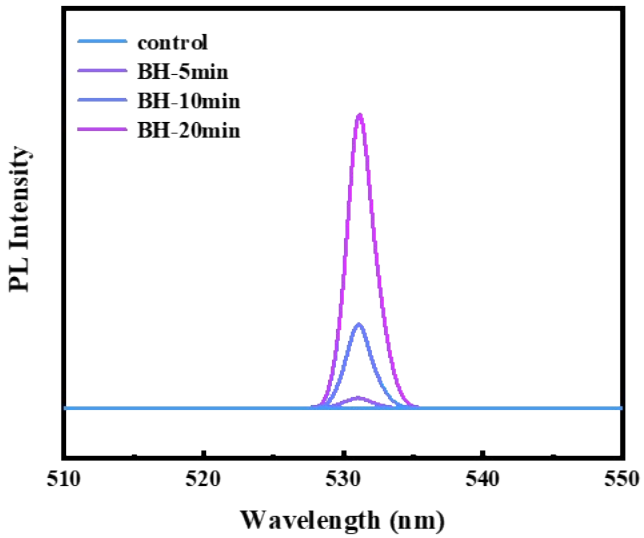


**Figure S12.** The steady-state PL of control and BH film.

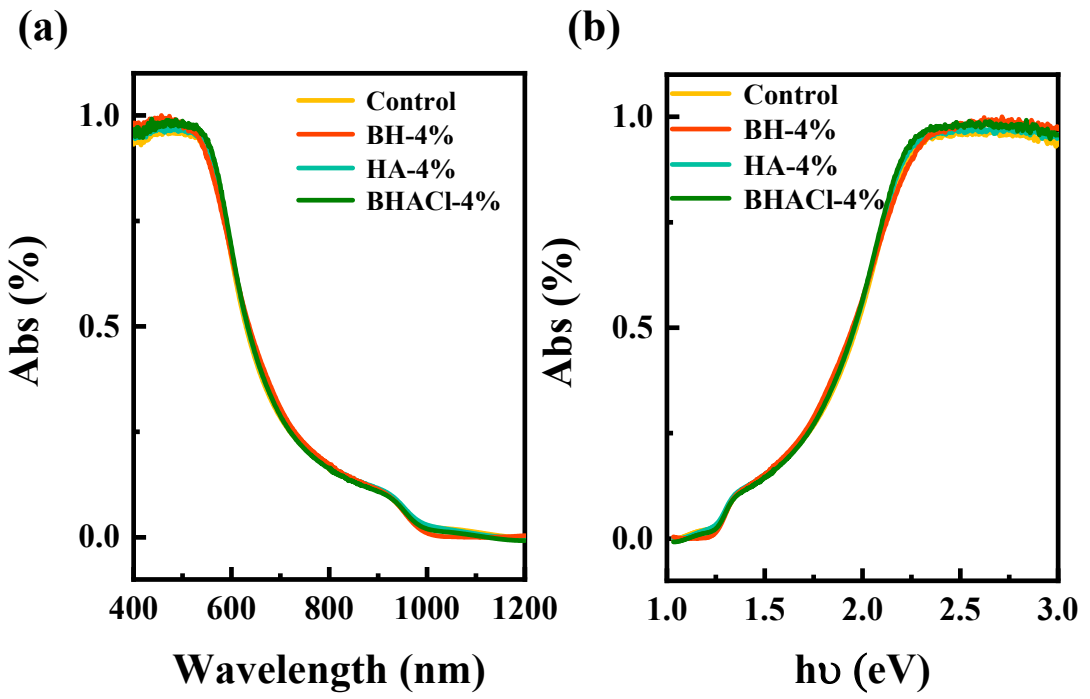


**Figure S13.** (a) The UV-vis absorption spectrum of control, BH, HA and BHACl film; (b) the Tauc' s plot calculated from the UV-vis absorption spectrum.

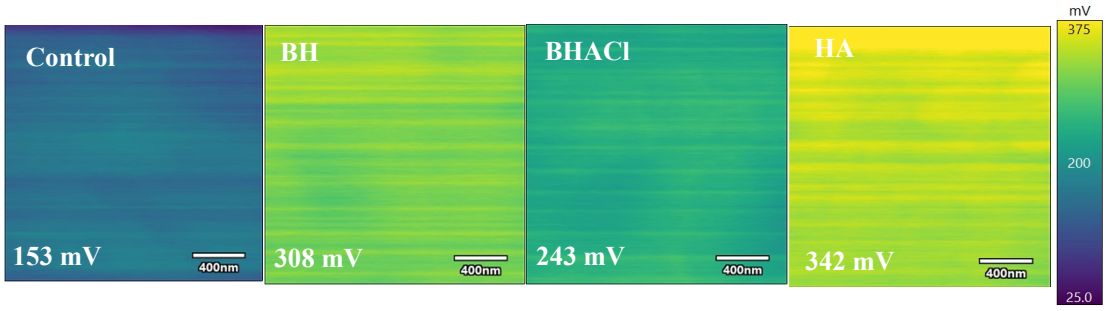


**Figure S14.** The KPFM of control, BH, HA and BHACl film.

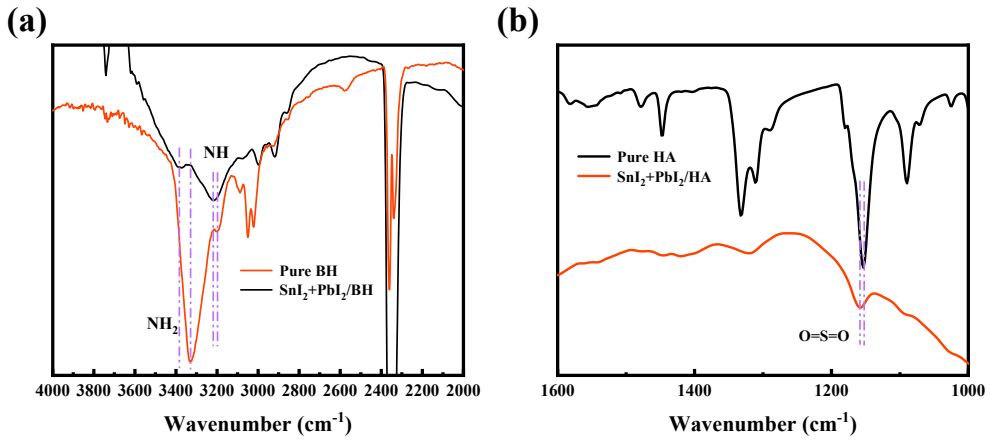


**Figure S15.** The FTIR of (a) BH film and (b) HA film.

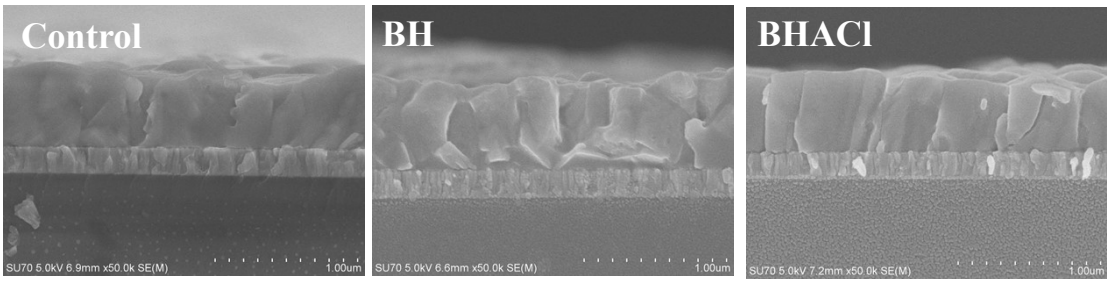


**Figure S16.** The cross-sectional SEM images of control, BH and BHACl film.

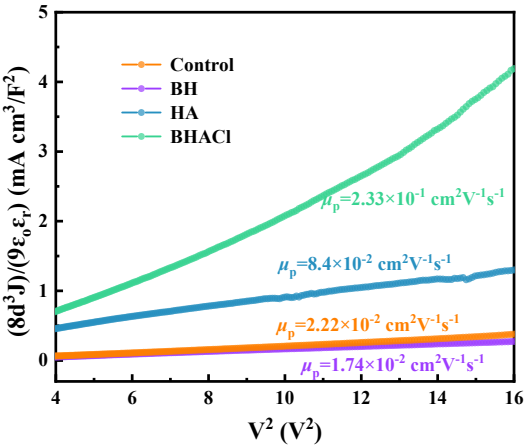


**Figure S17.** SCLC plots showing the hole mobilities (in unit of cm2 $V^{-1}$ $s^{-1}$) for control, BH, HA, and BHACl.

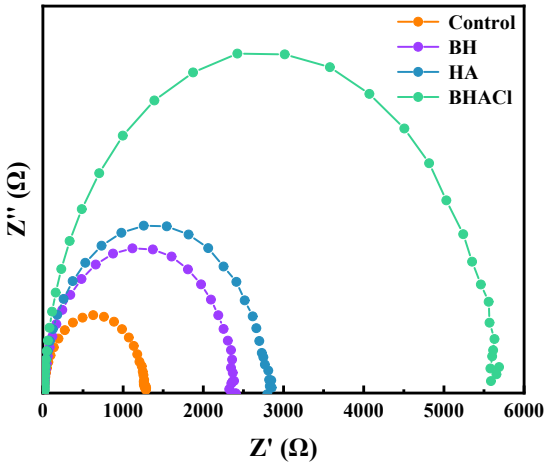


**Figure S18.** The EIS of control, BH, HA and BHACl devices.

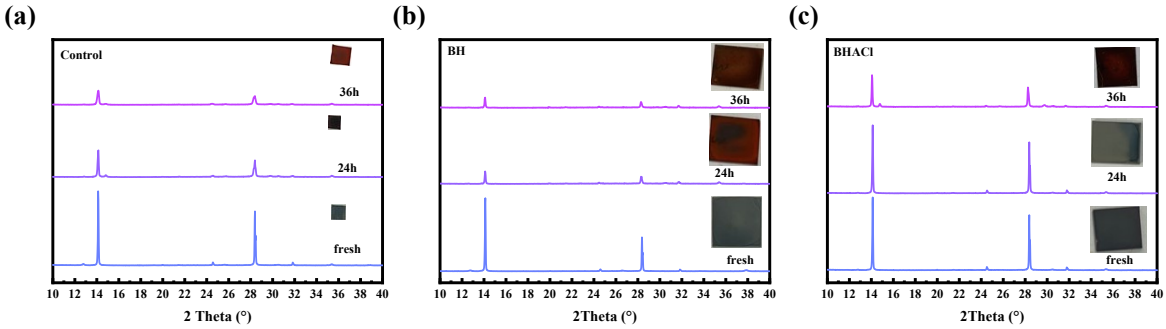


**Figure S19.** The XRD of (a) control film, (b) BH film and (c) BHACl film aged in air.